ELSEVIER

Journal of Chromatography A, 718 (1995) 239–255

JOURNAL OF CHROMATOGRAPHY A

Characterization of pore size distribution of packing materials used in perfusion chromatography using a network model

Kai-Chee Loh, Daniel I.C. Wang*

Department of Chemical Engineering, Biotechnology Process Engineering Center, Massachusetts Institute of Technology, 18 Vassar Street, Cambridge, MA 02139, USA

First received 21 March 1995; revised manuscript received 20 June 1995; accepted 21 June 1995

Abstract

A network model is used to represent the porous structure existing in a column packed with perfusive stationary phase. By matching model simulations with experimental mercury intrusion data, characteristics of the pore size distribution (PSD) of perfusive particles can be calculated quantitatively. It was found that the distribution is bimodal, consisting of an interconnected porous structure of macropores (pore diameters of the order of 1000 Å) and micropores (pore diameters of the order of 100 Å). Two different types of perfusive packings (POROS I and II) were compared in terms of capacity and throughput capabilities with respect to their PSD. The sensitivity and validity of the model was corroborated by simulating intrusion experiments on blends of the perfusive packings. The simulated results compared very well with the experimental data. The network model was used to elucidate pertinent parameters using perfusive packings such as surface area accessibility of various proteins and size-exclusion chromatography of polystyrene molecules. The agreement between experimental data and model predictions are excellent in both studies.

Keywords: Stationary phases, LC; Pore size distribution; Perfusion chromatography; Network model

1. Introduction

The current intense focus on perfusion chromatography for protein purification is due to its high separation speed. It has long been recognized that conventional high-performance liquid chromatography (HPLC) packed columns suffer from a number of limitations. The most important of these is the restriction to low flow-rates, which stems from the intrinsically low intraparticle diffusive mass transport.

In an effort to enhance the kinetics of the separation process, Afeyan et al. [1] have developed perfusion chromatography which takes advantage of packing materials with large through-pores (pore diameters of the order of 1000 Å). Under suitable conditions, a sufficiently high level of pressure-driven convective flow exists in these pores to augment the intraparticle mass transfer by convective transport. To circumvent the problem of low adsorption capacity due to low surface area, the large through-pores in the particles are intercalated with smaller

* Corresponding author. Address for correspondence: Room 20A-207, MIT, 18 Vassar Street, Cambridge, MA 02139, USA.

0021-9673/95/$09.50
SSDI 0021-9673(95)00706-7

diffusive pores (pore diameters of the order of 100 Å), resulting in a bimodal pore-size distribution (PSD) for these perfusive particles.

Theoretical analyses of the effects of intraparticle convection within these large-pore stationary phases have been developed with particular emphasis on the enhancement of column efficiency at high flow-rates [1–6]. These analyses have involved macroscopic modelling of the packing media and column properties which lump pore-structure characteristics (specifically the PSD) into the empirical tortuosity factor in the constitutive equations. Moreover, all of the models developed have assumed that the perfusive packings consist of a bimodal PSD where convection takes place in the macropores (through-pores) and diffusion in the micropores (diffusive pores). Although the characterization of pore structures of HPLC packing materials is important [7], especially when perfusion chromatography owes its success to the significantly different PSD of its packings compared to traditional diffusive stationary phases, to date, there has not been any data in the literature that characterizes perfusive particles with respect to their PSD (the relative proportions of macropores to micropores, the mean macropore and micropore diameter). This characterization is necessary in order to correlate the PSD of the particles to the performance of a column packed with such particles. In order to fully exploit the potential of large-pore packings in liquid chromatography, such understanding is definitely needed.

Porous packing materials have customarily been characterized in terms of PSD by methods such as nitrogen adsorption, mercury intrusion, size-exclusion chromatography (SEC) and transmission electron microscopy (TEM). In using the first three techniques, the traditional method of analyzing the resultant experimental data relies on the use of a "parallel-pore" model. In such a model, the porous structure of the particles is assumed to be a bundle of parallel cylindrical tubes of varying diameter but with the same length. The flaws in this approach are well documented [8] and are largely due to the fact that the parallel-pore model neglects the existence of the interconnections between the different pores in porous media. In the case of using TEM to characterize porous materials, Tanaka et al. [9] have found that TEM in combination with densitometric measurements can be used to visualize pore structures with the possibility to get a three-dimensional representation. Their method, however, is very laborious and it is not straightforward in providing a correlation between the characteristics of the porous structure and the performance of an HPLC column packed with the particles.

Discrete pore network models, which incorporate specific geometric properties of the pore space and also take into account the interconnections between the pores, have been developed to provide a more realistic representation of the pore space within porous media [10–13]. In such network models, the porous structure is represented by a lattice network (two-dimensional or three-dimensional) of nodes interconnected by bonds representing the pores. The network is generated using a Monte Carlo simulation approach whereby cylindrical pores are randomly assigned to the bonds of the network. In some models, known as pore-throat models [14,15], the porous structure is represented in the lattice network by large voids defined as spheres and narrow throats interconnecting the spherical voids defined as cylinders. Such models, however, have been criticized as being too restrictive, besides being not very realistic. Moreover, such network geometry makes it difficult to translate results to diffusion and reaction simulations. In constructing network models, the diameters of the assigned pores are distributed according to a PSD which has to be inferred by simulating mercury intrusion on the models and comparing the simulations to experimental data [12,16–18]. Variations of different network models have been used with great success for interpreting mercury porosimetry data and more realistically inferring the PSD of porous media. In addition, these models permit the direct study of transport phenomena within the pore space [13,19–21] and therefore facilitate the direct correlation of the effects of pore structure characteristics with the transport behaviour of the particles.

Our research has centred on establishing a

discrete pore network model to represent a perfusion chromatography column. This paper will provide, for the first time, characterization data on the PSD of perfusive packings, which will serve as a first stage in elucidating the relationship between pore structure characteristics and the performance of perfusive packings for use in HPLC. Simulation and experimental data will also be presented to compare different perfusive packings with regard to protein adsorption capacity and size-exclusion characteristics. It is important to emphasize that our contribution here is not in the development of a novel method but in the ability to predict and elucidate experimental observations using a well-established model at the network level.

2. Model formulation

The greatest challenge in pore structure modelling is to incorporate the elements of randomness and chaos implicit in porous media in such a way as to retain both structural realism and tractable quantitative treatment. In our work, the packed column is represented by a cubic lattice network of interconnected cylindrical pores. Cylindrical capillary geometry is used because of tradition and convenience in the calculation of the effective diffusivity and other related transport phenomena properties. The lattice used consists of a regular ($X \times Y \times Z$: $L \times L \times L$) array of nodes connected to each other by bonds of the network (Fig. 1). To represent the porous media in the column realistically, the bond-size distribution of the network should be similar to the PSD existing in the chromatographic media. The porous structure in the HPLC column is classified into two classes of pores–interstitial pores, representing the pores between the bead particles, and intraparticle pores, representing the pores within the porous beads: the latter being subdivided into two subclasses of pores–macropores and micropores. The "composite" pore-size distribution representing the porous structure is represented topologically in the lattice shown in Fig. 1 by randomly assigning cylindrical pores to the bonds in the network. Here, the nodes are assumed to have no volume in the network.

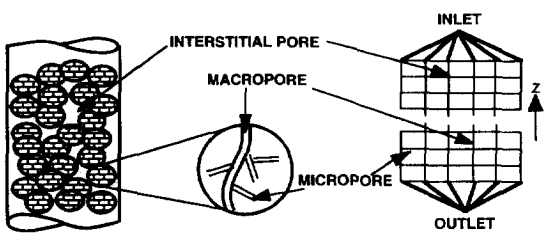

Fig. 1. Schematic representation of chromatographic media for network model.

Basically, a point in the network (coordinates x, y, z) is selected at random and an orientation of the pore is chosen (orientation pointing to the left, to the front or downward from the node). In this case, only three orientations need be considered as the other three orientations at a cubic network node will be accounted for by nodes adjacent to the node in question. This cylindrical pore is then assigned a diameter based on a predetermined statistical distribution function representing the PSD. The type of distribution function to use was determined by performing digital image analyses on scanning electron microscopy (SEM) images of the external surfaces of the perfusive particles. Although the porous structure at the external surfaces could be different from that existing internally, it has been reported [22–25] that, in general, the overall PSD of the particle is correlated to the porous structure of the external surfaces. Frequency data of particle and macropore sizes were obtained from the image analyses and probability plots were made. Fig. 2 shows that frequency data of particle and macropore sizes correlate very well with the Gaussian distribution, as evident from the straight-line plot obtained. However, at much higher magnifications on the SEM, the images obtained were not sharp enough for image analysis to be performed for the micropores. There is no reason, nonetheless, for the distribution function describing the micropore sizes to be different from that describing the macropore sizes. Hence, a Gaussian distribution is also used to represent the micropore sizes. Although the PSD used in this work is predominantly the Gaussian distribution function, the network model can be generated using

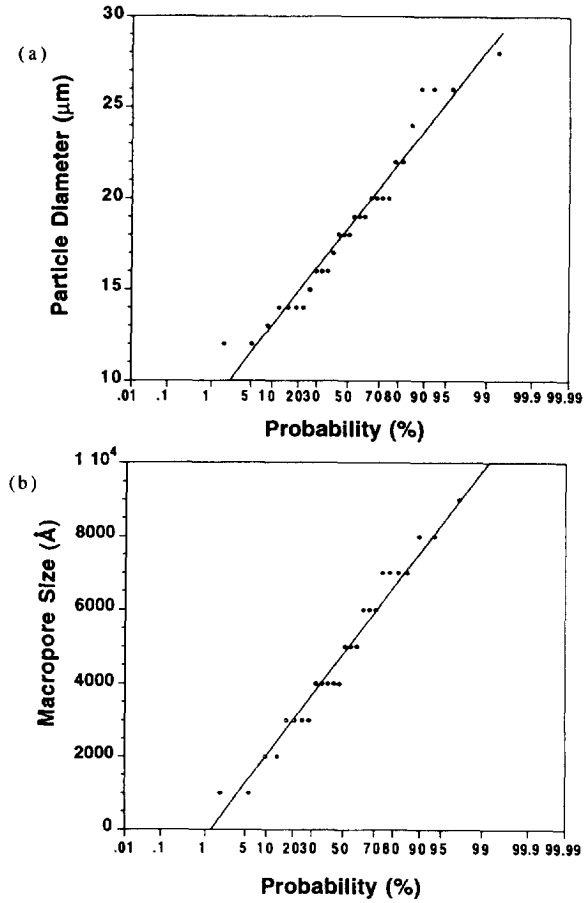

Fig. 2. (a) Probability plot of particle size distribution of POROS I. (b) Probability plot of macropore size distribution of POROS I.

any other statistical distribution functions depending on the actual porous structure.

The PSD used in the network is hence made up of the sum of three Gaussian distributions to represent the three types of pores present in the column (as mentioned earlier):

$$\mathrm{PSD}(D) = \sum_{i=1}^{3} \frac{P_i}{\sqrt{2\pi}\sigma_i} \exp\left[-\frac{1}{2}\left(\frac{D-\mu_i}{\sigma_i} \right)^2 \right] \quad (1)$$

where PSD is the pore-size distribution, P_i the relative proportion of pores of class i, μ_i the mean diameter of pores of class i, σ_i the standard deviation of the diameter of pores of class i, and D the diameter of pores.

In our model, a three-dimensional network is used since only in three dimensions is it possible to have two continuous phases present simultaneously. In two-dimensional networks, one phase can be continuous–the second must be discontinuous. It is the generally accepted view that in actual porous media there is a range of saturations where at least a portion of each phase is continuous [9]. Hence, two-dimensional networks cannot be used to accurately model actual porous media. Moreover, with the help of supercomputers like the CRAY Y-MP, highly intensive and complex calculations can be handled even when resorting to three-dimensional models. For full details on the computational methods used here, the reader is referred to the Ph.D. thesis by Loh [26].

At the surfaces of the lattice, periodic boundary conditions are applied for the x- and y-directions. These boundary conditions are used so as to take into account end effects and finite-size modelling [27]. As for the z-direction, pores on the top and bottom surfaces are assigned the downward orientation only. The procedure for selecting a pore and assigning a diameter is continued until a predetermined number of pores have been added. The number of pores added determines the pore-interconnectivity (PI) of the porous structure. The PI is defined as the average number of bonds connected to each node. Interconnectivity can have a tremendous impact on transport processes in porous media. For low values of the PI, there may be no open pathway for molecules to move within the media, while at high values of PI, multiple pathways may exist. Here, constant network connectivities will be considered, although in general a connectivity distribution can be specified for the network.

In Monte Carlo simulations, the use of an appropriate random number generator is very important in order that the representations are realistic. Here, the pore coordinates and pore orientation are chosen using a non-biased uniform number generator. In the case of pore diameter, a PSD-specific generator [28] is more appropriate. Pore diameters are selected from the corresponding PSD according to the relative

probability of abundance of each pore in the distribution.

The bond length used in setting up the lattice network can be constant, randomly assigned, or related in some manner (directly or inversely proportional) to the diameter. Photomicrographic studies have shown, however, that the length of a pore is of the same order of magnitude as its diameter [8]. Different studies [11,20,29,30] have assigned lengths to the bonds by different methods. Although sensitivity analyses [13] and the network simulations of porous media made by the above-mentioned workers have demonstrated that network model predictions for transport properties based on all the various methods agree well with experimental observations, at the present time, it is unclear as to which of these alternative tends to be most naturally prevalent in porous media. However, it seems likely that larger-diameter pores will tend to be associated with larger pores rather than the reverse. In our model, a pore length equal to the diameter of the pore is used.

In a column which is formed by the packing of micro-porous beads, there are two distinct classes of void structures; interstitial and intraparticle pores are correlated and therefore cannot be assigned to the network randomly [19]. If pore sizes are assigned to the network from widely differing distributions in an uncorrelated manner, the network generated will be such that there will be pore-shielding of some of the interstitial pores by the smaller intraparticle pores, which will then be an unrealistic representation of the porous structure existing in the column. In a representative section of the column, the interstitial voids form a percolating pore cluster, which in turn connects the highly interconnected intraparticle voids. Hence, to generate a realistic network representation of the column, the interstitial voids are assigned in a "semi-random" manner to a percolating cluster which transects the lattice. Although the diameters of the interstitial pores are assigned randomly from the predetermined PSD, the pore position and orientation are partially randomly selected in such a manner that the interstitial pores are connected in the percolating cluster. As for the intraparticle pores, assignment of pores in the network is completely random to simulate the isotropicity of the particle pore structure formed from polymerization.

3. Mercury intrusion simulation

Once the network has been constructed, the process to simulate mercury intrusion is first initiated. By comparing the simulated intrusion curve with the experimental data, the pore size distribution used to generate the network is adjusted until there is a good fit between the two curves. The adjustment is made by systematically changing the parameters which define the PSD. The goodness-of-fit between simulations and experimental data is assessed by a parameter similar to the chi-square factor [31]. This will be described later. In this way, the PSD of the perfusive particles is inferred through an iterative trial and error computational procedure. In addition, matching the simulated and experimental curves will incorporate the relevant porosities inherent in the actual porous structure in the network model. Mercury intrusion on the network is simulated using the algorithm shown in Fig. 3 and is modelled after Lane [32]. Initially, the void space is assumed to be evacuated. The program starts by incrementally increasing the pressure, emulating the actual experimental procedure. In mercury porosimetry, the Washburn equation (Eq. 2) is used to relate the intrusion pressure to the diameter of a cylindrical pore:

$$P = \frac{-4\gamma \cos\theta}{D} \tag{2}$$

where P is the intrusion pressure (psia), γ the surface tension of mercury (485 dynes/cm), θ the contact angle between mercury and pore surface (140°), and D the pore diameter (Å).

Incrementally increasing the pressure can be accomplished by the equivalent process of decreasing the critical diameter for intrusion according to Eq. 2. The first pores to be filled are the interstitial pores in the percolating interstitial cluster. These provide the mercury menisci

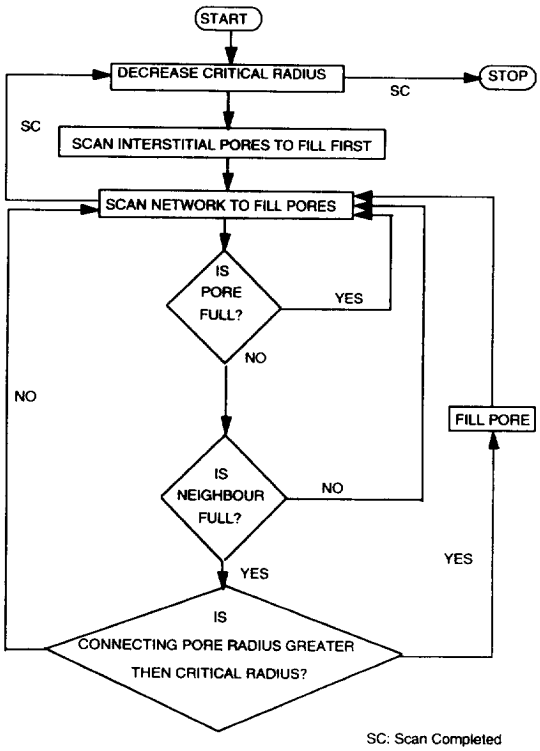

Fig. 3. Flow chart for mercury porosimetry simulation.

necessary for mercury penetration into the microporous structure of the beads.

The network is scanned to intrude pores based on a number of criteria. A pore will be filled if (1) the pore is empty, (2) at least one of the pore's neighbours is filled, and (3) the diameter of the empty pore is at least equal to the current critical pore diameter. Upon satisfying the above conditions, the pore is filled with mercury and the network is scanned again at the same critical diameter until no further pores can be filled. The cumulative volume of mercury that has intruded into the void space at that pressure (critical diameter) is then recorded. The critical diameter is then gradually decreased and the intrusion process repeated until the size of the smallest pore in the network is reached.

In matching the simulated and experimental intrusion curves, the sum of squares of the residuals, given by Eq. 3, is used to test the goodness-of-fit, F:

$$F = \sum_i \left(\frac{y_{i,\mathrm{sim}} - y_{i,\mathrm{expt}}}{y_{i,\mathrm{expt}}} \right)^2 \quad (3)$$

where $y_{i,\mathrm{sim}}$ is the pressure at simulated intrusion volume V_i, and $y_{i,\mathrm{expt}}$ is the experimental pressure at the same intrusion volume V_i.

The F factor defined in Eq. 3 is similar to the chi-square (χ^2) factor used in statistical analysis [31]. Note that the lower the F factor, the better is the fit between simulation and experimental data. The pressures were used in the F factor since the pressures vary in a logarithmic fashion while the intrusion volume varies linearly. Hence, minimizing the errors in the pressure will inherently minimize the errors in the intrusion volume.

The goodness-of-fit, F factor, gives the total fractional error of the closeness of fit between the simulated and the experimental curves, and the objective is to adjust the inputs of the lattice network (parameters in the PSD and the PI) such that a minimum F is achieved.

4. Adsorption capacity simulation

It can be shown and derived from principles of statistical mechanics that the exclusion probability, $E(r)$, of a solute in a pore depends on the size and shape of the solute molecules and on the size and shape of the pores in the column packing material [33]. For the case of a solute molecule which can be taken as a "hard sphere" of radius r and the pore an infinite cylinder of radius R, it follows from steric interactions [34] that the center of mass of the molecule cannot approach any closer than a distance r from the wall of the pore and the part of the pore volume which is accessible to the center of mass of the solute is a cylinder of radius $(R - r)$.

As a consequence, the exclusion probability, which is the probability that a pore is accessible to the molecule, can be presented as:

$$E(r) = \left(1 - \frac{r}{R}\right)^2 \quad \left(\frac{r}{R}\right) < 1,$$

$$E(r) = 0 \quad \left(\frac{r}{R}\right) > 1.$$

Based on this relationship, the accessibility of a protein molecule in a cylindrical pore can be assessed in the network model to simulate the adsorption capacity of the perfusive particles for different proteins. For the lattice network, the total accessible area for adsorption can be obtained from:

$$A(r) = \sum_{R=r}^{R=\infty} \left(1 - \frac{r}{R}\right)^2 4\pi r^2 \quad (4)$$

since the pore length is the same as the pore diameter in the network.

Using the same algorithm as that used in simulating mercury intrusion, with the critical diameter representing the diameter of the protein, the process of protein adsorption can be simulated on the network model. Here, each time a pore is accessed, the total accessible area is calculated from Eq. 4 to represent the adsorption capacity.

5. Size-exclusion chromatography simulation

Size-exclusion chromatography (SEC) has been mainly employed as an analytical procedure for separating macromolecules according to differences in size. While simulating protein adsorption on the network model predicts experimental data based on the surface area of the packing beads, simulating SEC will elucidate experimental results based on the volumetric porosity of the particles. Different models have been proposed to evaluate the partition coefficient, K, of flexible-coil macromolecules between the bulk solution and cylindrical pores [33,35,36]. By using a Monte Carlo simulation technique, Davidson et al. [36] provided a simple and most complete relationship which relates the partition coefficient to the radius of gyration of a flexible-coil macromolecule:

$$\ln K = \ln K_0 + (l/R)(0.49 + 1.09\lambda_G + 1.79\lambda_G^2) \quad (5)$$

where K is the partition coefficient, $K_0 = 4\Sigma_{i=1}^{\infty}(1/\alpha_i^2)\exp(-\alpha_i^2\lambda_G^2)$, $\lambda_G = r_g/R$ is the ratio of radius of gyration of macromolecule to pore radius, α_i are the roots of the Bessel function of the first kind and of order zero, l is the segment length of the macromolecule, given by: $r_g = l\sqrt{(n^2-1)/(6n)}$, where n is the number of segments.

For the lattice network, the partition coefficient for different polystyrene molecules can therefore be obtained as:

$$K(r_g) = \sum_{R=r_m}^{R=\infty} F(R)K(R)$$

where $F(R)$ is the accessible volume fraction of pores in the network taken up in radii R.

Hence, using the same algorithm as that used in simulating mercury intrusion, with the critical diameter representing the diameter of gyration of the polystyrene molecule, size-exclusion chromatography can be simulated on the network model.

6. Materials and method

6.1. Mercury porosimetry

Mercury intrusion experiments were conducted using a Micromeritics PoreSizer 9320 porosimeter (Micromeritics, GA, USA). Measurements were made over the pressure range from 1 to 30 000 psia. The samples used were POROS R1M and R2M supplied by PerSeptive Biosystems (Cambridge, MA, USA). In this paper, these two media will be referred to as POROS I and POROS II, respectively. These are 20-μm particles used for reversed-phase chromatography. For each experiment, 0.1 g of the sample was used. The mercury advancing contact angle used was 140° and the surface tension of mercury was taken to be 485 dynes/cm.

6.2. Protein adsorption capacity

Static experiments were carried out by mixing 20 mg of the chromatographic particles with different concentrations of protein solutions (0.5, 1.0, 2.0 and 4.0 mg/ml) to obtain the adsorption

isotherm. The proteins used in the experiments were all obtained in purified form from Sigma Chemicals (St. Louis, MO, USA). Their relative molecular masses and effective solute diameter (calculated based on diffusivity measurements) are tabulated in Table 1. Before mixing with the protein solutions, the particles were wetted with 40 μl of isopropyl alcohol, which was subsequently centrifugally removed by diluting with 2 ml of water. The suspension of particles and protein solutions was mixed using an orbital shaker overnight and the unbound protein remaining in solution was measured using UV detection at 280 nm. The amount of bound protein was calculated from a material balance. In order to check the validity of using material balance as an accurate measure of the amount of protein adsorbed on the media, the bound protein was eluted from the particles with 20% acetonitrile (ACN) in 0.1% trifluoroacetic acid (TFA)–water and the eluted protein concentration detected using the UV spectrophotometer. This was performed only for lysozyme, since this protein elutes cleanly from the particles. The error in using the material balance to calculate the amount of bound protein was found to be less than 7%. In all subsequent experiments, the proteins were therefore not eluted and the material balances were used to assess protein adsorption.

The adsorption isotherms obtained experimentally were fitted with Langmuir–Hinshelwood adsorption kinetics to obtain the maximum static capacity for each protein:

$$q = \frac{q_{max} S_{eq}}{K_p + S_{eq}} \tag{6}$$

Table 1
Properties of proteins used in protein adsorption studies

Protein	Molecular mass (× 1000)	Radius (Å)
Lysozyme	14	24
Ovalbumin	45	36
Hemoglobin	68	41
Transferrin	77	43
Fibrinogen	340	71

where q is protein adsorbed (mg/ml), q_{max} maximum static capacity (mg/ml) , S_{eq} equilibrium protein concentration (mg/ml), and K_p the affinity constant of protein for the particle surface (mg/ml).

6.3. Size-exclusion chromatography (SEC)

SEC was performed on the Hewlett-Packard HP1090L system (Waldbronn, Germany). The chromatographic media used were R1M and R2M packed in columns of 100 × 4.6 mm I.D. The polystyrene standards (Supelco, PA, USA) were prepared in HPLC grade tetrahydrofuran at 0.1% w/v. Properties of the polystyrene standards are tabulated in Table 2.

The flow-rate for the HPLC studies was 0.40 ml/min and the eluate was detected at a wavelength of 220 nm.

The solute diameters of the polystyrene standards can be obtained from the formula [37]:

$$D(\text{Å}) = 0.246\, M^{0.588} \tag{7}$$

where M is the relative molecular mass of the polystyrene molecule. The diameters of the polystyrene standards used in the experiment were calculated from Eq. 7 and are shown in Table 2.

The exclusion coefficient, K, at each solute diameter, can be calculated as follows: Volume of column is V_c, total volume of pores in column is $\epsilon_t V_c$, volume of interstitial pores $V_0 = \epsilon_c V_c$ and volume of intraparticle pores $V_i = (\epsilon_t - \epsilon_c)V_c$. This gives for the exclusion coefficient

Table 2
Polystyrene standards used in size-exclusion chromatography

Molecular mass (× 1000)	Polydispersity	Diameter (Å)
7.5	1.06	46
25	1.06	94
47.5	1.06	138
90	1.04	202
207	1.06	328
900	1.10	780
3000	1.20	1584
6000	1.12	2380

$$K = \frac{V_e - V_0}{V_i} \quad (8)$$

where V_e is the elution volume of polystyrene solute, ϵ_t total porosity in the column (interstitial + intraparticle pores), and ϵ_c the column porosity.

7. Results and discussion

7.1. Mercury intrusion of POROS I and POROS II

It is necessary to determine the transition between interstitial and intraparticle pore sizes in the simulation of mercury intrusion for the network model. This is because the interstitial pores provide the mercury interface necessary for mercury penetration into the network.

The transition from interstitial to intraparticle pore size is determined from a comparison of the intrusion curves of POROS I and POROS II (Fig. 4). From Fig. 4, it can be seen that the departure of the intraparticle pores between the two media occurs at approximately 1.0 μm. Hence, 1.0 μm is taken to be the cutoff between interstitial and intraparticle pores.

The computer simulations were performed on the CRAY Y-MP supercomputer, which takes approximately 300 s to perform each simulation of the mercury porosimetry experiment. Parameters of the PSD and PI were first obtained for POROS I from the simulations. Since the particle size distributions for POROS I and II are essentially the same (SEM and image analyses data), the same distribution function describing the interstitial pores in POROS I should apply to POROS II. Moreover, the PI of the porous structure comprising POROS I can be taken to be the same as the PI of the porous structure comprising POROS II, since the two packings are manufactured similarly. In the case of POROS II, therefore, there are four less parameters in the PSD function to be inferred from the mercury porosimetry simulations.

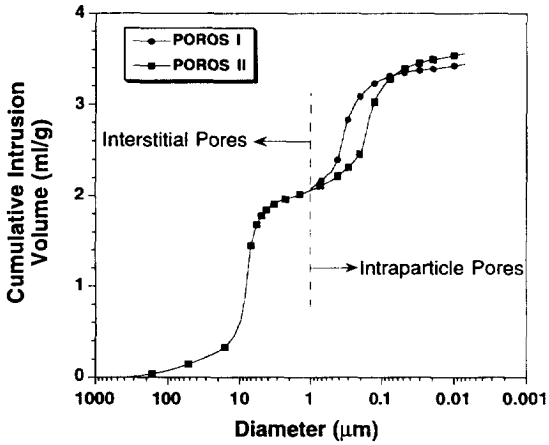

Fig. 4. Relationship between pore diameter to cumulative intrusion volume for POROS I and II obtained by mercury porosimetry. Dotted line indicates cutoff point between interstitial and intraparticle pores.

Figs. 5a and 5b show a comparison of the intruded volume of mercury as a function of pressure for the simulations and experimental data for POROS I and II, respectively. Since the network model is used to represent a finitely small section of the column, several independent realizations of the system have to be generated. The simulated intrusion curve obtained from a single realization will be "jagged" in character and is unique to the particular set of random numbers used in generating the model. A realization is defined as the different networks generated using different selections of random numbers to account for statistical variations. The number of realizations needed usually depends on the size of the sample and on the desired accuracy. For large samples, a few realizations often provide accurate estimates of the quantities of interest. Since we are modelling a very small sample of the column, 50 realizations were carried out, so that one standard deviation from the stochastically averaged simulated curve is less than 10%. In the figures, the average simulated curve is shown and error bars represent one standard deviation from the mean values.

By adjusting the PSD and PI used in generating the network, the experimental and simulation data were matched to an F factor of less than 1.00 for both POROS I and II. This F factor corresponds to an average fractional error of less than 10% for the 92 experimental data

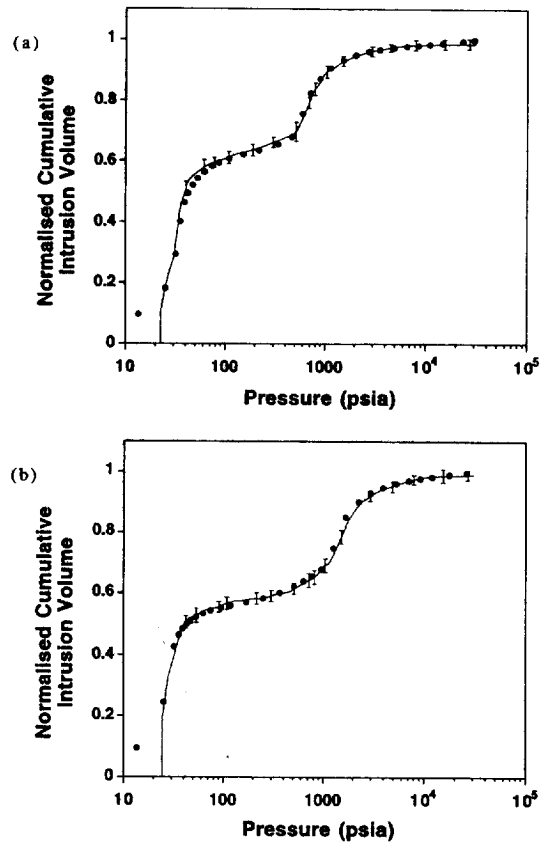

Fig 5. Comparison between simulated and experimental intrusion curves: (a) POROS I, (b) POROS II. Simulation data represent the average of 50 realizations and error bars indicate 1 standard deviation from the mean. (●) Experimental data, (line) simulation data.

points. The only exception in agreement between the simulated and experimental data is a very short segment at the early stage of the experimental intrusion curve, which represents the filling of the void space in the sample holder during the porosimetry experiment. This part of the curve is therefore not representative of pore space existing in the HPLC column.

A summary of the parameters for the PSD used in the simulations is tabulated in Table 3. From the simulations, it was found that the porous structure of the perfusive particles, POROS I and II, indeed consists of an interconnected porous structure of two groups of widely differing pore sizes; a group of large pores (of the order of thousands of angstroms in sizes), through which convection is believed to take place, and a group of small pores (of the order of hundreds of angstroms in pore sizes), where diffusion occurs. These results are consistent with the approximate measurements of the pore sizes by Afeyan et al. [1] inferred from scanning electron microscopy. They have reported macropore sizes of about 6000–8000 Å interconnected by diffusive pores of about 500 Å. Moreover, a comparison between POROS I and II shows that POROS II has an abundance of smaller pores, in both the macropore and micropore sizes (evident in the relative proportion of micropores to macropores), compared to POROS I, which effects a higher amount of

Table 3
Summary of parameters of pore size distribution for POROS I and II

	POROS I			POROS II		
	p_i	μ_i	σ_i	p_i	μ_i	σ_i
Macropore	1.0	5000 Å	2100 Å	2.8	3500 Å	2000 Å
Micropore	0.35	250 Å	450 Å	0.98	160 Å	280 Å
Interstitial	0.21	5.6 μm	1.82 μm	0.21	5.6 μm	1.82 μm
PI	2.5			2.5		

The parameters used here are the same as those defined in Eq. 1, where p_i is relative proportion of pores of class i, μ_i mean diameter of pores of class i and σ_i standard deviation of diameter of pores of class i.

surface for adsorption (about 40% more in POROS II compared to POROS I).

Also found from the simulations is the magnitude of the mean pore size of the interstitial pores in the column: a mean size of 5.6 μm was obtained. This corresponds to a ratio of pore size to particle diameter of $5.6/20 = 0.28$. In reports of particle-size analysis using mercury intrusion measurements, various researchers [38–40] have used different sphere-packing models to elucidate the mean size of the pore spaces between packed spherical particles. They have found that the ratio of the mean size of the pores between these particles to the diameter of the particles ranges from 0.27–0.37 depending on the porosity of the packing. Our results is therefore consistent with the values reported in the literature.

To investigate the uniqueness of the PSDs obtained from the simulation matches, sensitivity analysis of the input parameters of the model was performed and it was found (data not shown) that the results in Table 3 are unique. The results presented so far provide, for the first time, a characterization of the porous structure existing in perfusive particles, using a model at the microscopic level. In what follows, data will be presented to show that experimental data pertaining to the surface area and porosity of the particles can be elucidated from the network model without the use of adjustable parameters. Before this is done, it is necessary to study the effects of the size of the lattice on the simulation results.

7.2. Effects of lattice size

It is obvious that every computer uses finite computational time and has finite storage memory. While using networks of larger lattice sizes may be more valid for representing an actual porous medium, larger networks suffer from having computations which become cumbersome and in some cases intractable, even with the most powerful computers. On the other hand, one has to be careful about how the simulation results are extrapolated to the asymptotic limits of an infinite system. One way to deal with finite-size simulations is the use of periodic boundary conditions, which have been used in our networks. Still, it is necessary to investigate the effects of lattice size on the simulation results. The mercury intrusion simulations for POROS I were performed on cubic networks of $L \times L \times L$ lattice sizes for L ranging from 10 to 30. For each lattice network, the average goodness-of-fit, the F factor, was obtained for 20 realizations and the results are plotted against lattice size, L, as shown in Fig. 6. Numbers next to the data points represent the average fractional error in each simulation.

It can be seen that although smaller lattice sizes require much less computational time and memory, the errors involved in the simulations are concomitantly higher. On the other hand, there is not a clear advantage in using large networks ($L = 30$ compared to $L = 25$) in terms of the goodness-of-fit. The CPU time necessary for the $L = 30$ networks compared to the $L = 25$ networks is about 75% more. For all simulation work presented here, a lattice size of $25 \times 25 \times 25$ was used.

7.3. Discretization of pore number distribution

In the presentation on the PSD so far, the discussion has been limited to the relative parameters of the distributions: namely the mean and standard deviation of the distribution. It will

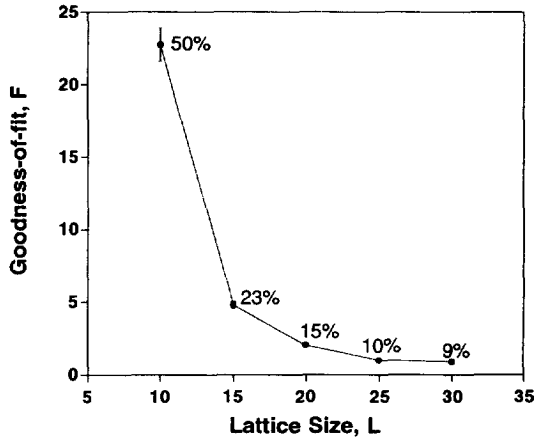

Fig. 6. Effects of lattice size on goodness-of-fit based on average of 20 realizations. Numbers next to data represent average error from 92 experimental data points.

be very useful if the number of pores in the respective groups of pores can be obtained on a per particle (or per unit particle volume) basis. This will not only serve as a good indicator of the pore sizes and relative number abundance of the pores, but it will also facilitate an efficient comparison between different perfusive particles. Since the model used in this research is fundamentally a discrete representation of the porous media, it is possible to discretize the pore number distributions for both POROS I and II. The discretization results are shown in Fig. 7. In this figure, the number of pores per bead particle is plotted as a function of pore diameter. Similar plots for number of pores per unit bead volume as a function of pore diameter can also be obtained, for comparing particles of different sizes. Since the samples used in our study are both 20 μm in diameter, the ordinate of number of pores per bead is a sufficient comparison.

As seen from Fig. 7, the number of pores in POROS II is as much as three-fold greater than that in POROS I for the pore sizes ranging from 20 Å to approximately 5000 Å. This was intentionally included by the manufacturer to effect more surface area for protein adsorption in the case of POROS II. It must be made known at this point that the porosities for both POROS I and II are similar, at about 60%. At a first glance of the data, there seems to be a contradiction in terms of the porosities of the two media.

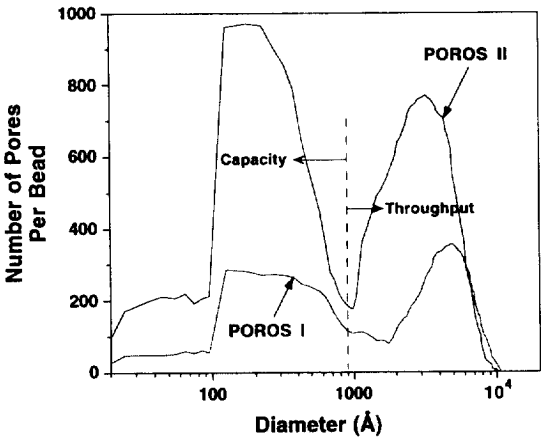

Fig. 7. Pore number distribution discretized on a per particle basis for POROS I and II.

The apparent question being how is it possible for POROS II to have an as much as three-fold higher number of pores compared to POROS I and yet maintain the same porosity? The answer lies in the pore diameter range between 7000 and 10 000 Å. It is important to recall that the volume of the pores is directly proportional to the cube of their diameters. Therefore, despite the fact that there are three times more pores for POROS II in the smaller and broader diameter range, the two- to three-fold more pores for POROS I in the larger diameter range, albeit narrower, more than make up for the apparent differences in porosities of the particles.

More importantly, the results demonstrate the applicability of the network model to semi-quantitatively compare the performance (in terms of adsorption capacity and throughput) between the two perfusive packings. The pore number distributions shown in Fig. 7 can be divided into two parts–one in the pore diameter range from 20 to 1000 Å, and another in the range from 1000 Å to about 1 μm. The first part represents the diffusive micropores and this assesses the adsorptive capacity of the particles while the second, representing the convective macropores, assesses the throughput of the particles. Keeping the same particle porosity, the higher abundance of micropores in POROS II compared to POROS I provided more adsorptive capacity while maintaining the mechanism of perfusion chromatography (high throughput at low pressure drop) by having sufficient macropores in the particles. This explains the better performance of POROS II compared to POROS I.

7.4. Mercury intrusion of blends of POROS I and II

To demonstrate the use of the network model to predict experimental results based on mercury porosimetry, samples of POROS I and II were blended in various proportions (25%, 50% and 75% of POROS I in the blends) and mercury intrusion experiments were performed on the resulting samples. Using the input parameters independently obtained for POROS I and POROS II, lattice networks were generated for

the blends and simulations of mercury intrusion into the networks were carried out. Simulation and experimental results are compared in Fig. 8 for the different blends. Again, 50 realizations were performed for each of the simulation experiment. With no adjustable parameters, it was possible to obtain an excellent agreement between the experimental and the simulation data for all the three blends. The goodness-of-fit ranged from 1.32 to 1.80, corresponding to average fractional errors of only 12 to 14%. An important implication of this is the possibility of using the model for quality control and quality assurance applications. For a random batch of the stationary phase from the production line, it is now possible to determine if the porous structure manufactured is within specifications by not just simulating the pure-sample intrusion but also blends of the random batch with known, characterized batches and comparing the simulated data with experimentally obtained data.

7.5. Protein adsorption capacity studies

In an effort to investigate the application of the model to elucidate surface accessibility of the media, experiments on equilibrium adsorption capacity were performed on POROS I and II for proteins of various molecular masses and hence molecular sizes. Fitting the Langmuir–Hinshelwood kinetics to the adsorption isotherms, the maximum static capacities and the affinity constants for the various proteins on POROS I and II were obtained. These are tabulated in Table 4.

Fig. 9 plots the absolute protein capacities for the two packings. For all proteins studied, it can be seen that POROS II provides more accessible area for adsorption compared to POROS I. In comparing the accessibility of adsorption surface area as a function of the protein size, however, the ratio of adsorption capacity of POROS II to I is more meaningful than the absolute static capacity. In using the ratio, surface chemistry between the proteins and the adsorptive surface can be eliminated and protein accessibility can be evaluated on a wholly physical basis. This will be possible if the particles under comparison have the same surface chemistry with respect to

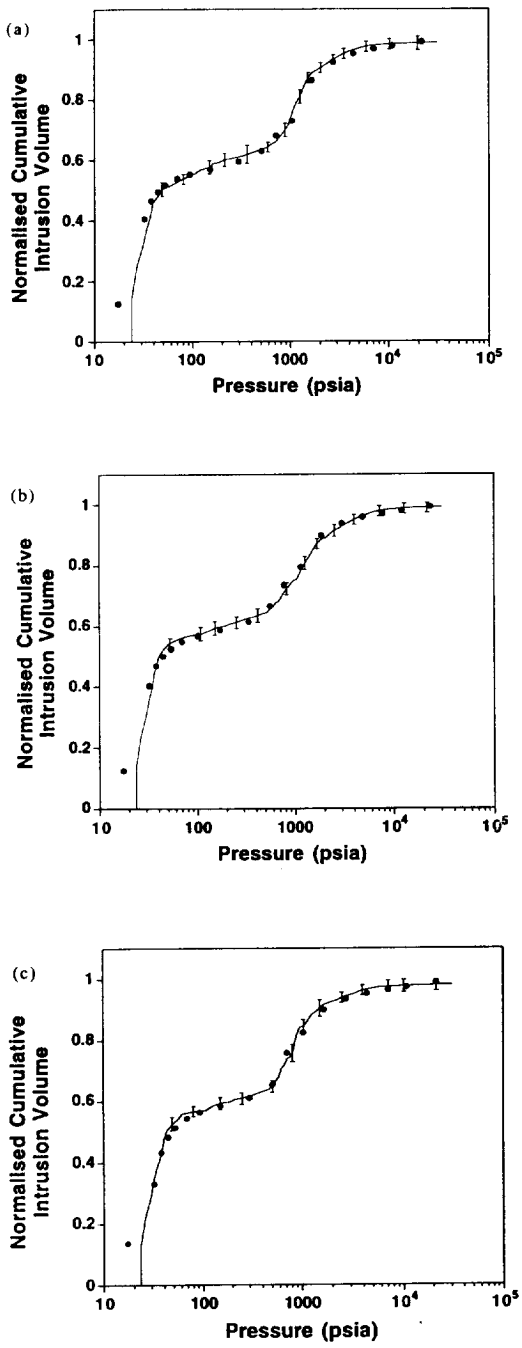

Fig. 8. Comparison between simulated and experimental intrusion results of blends of POROS I and II. (a) 25/75% POROS I/II; (b) 50/50% POROS I/II; (c) 75/25% POROS I/II. Simulation data represent average of 50 realizations and error bars indicate 1 standard deviation from the mean. (●) Experimental data, (line) simulation data.

Table 4
Parameters of Langmuir–Hinshelwood adsorption isotherm

Protein	POROS I		POROS II		$q_{max,II}/q_{max,I}$
	K_p	q_{max}	K_p	q_{max}	
Lysozyme	2.065	20.54	1.924	28.55	1.39
Ovalbumin	2.709	40.57	2.695	55.18	1.36
Hemoglobin	0.721	35.80	0.606	47.97	1.34
Transferrin	0.086	16.40	0.101	21.81	1.33
Fibrinogen	0.011	58.89	0.013	75.38	1.28

The parameters used here are the same as those defined in Eq. 6, where q_{max} is maximum static protein capacity of the media (mg/ml) and K_p affinity constant of protein for media surface (mg/ml).

the proteins under examination. From Table 4, it can be seen that the K_p values obtained for POROS I and II are comparable, with a maximum difference of only 15%. It can hence be concluded that POROS I and II both have the same surface chemistry for each of the proteins used in our study, and the assumption of equating the ratio of the protein capacities to the ratio of the accessible surface areas of the particles is therefore justified.

Using the solid sphere model, accessible surface areas of the packings were simulated as a function of protein size. A plot of experimental and simulated results is shown in Fig. 10. For

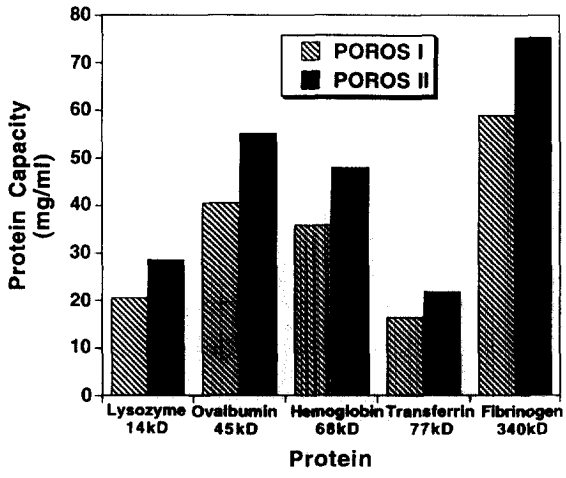

Fig. 9. Equilibrium protein adsorption capacity for POROS I and POROS II with proteins of different molecular masses.

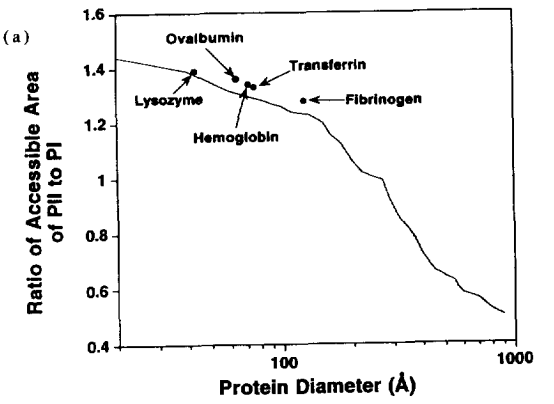

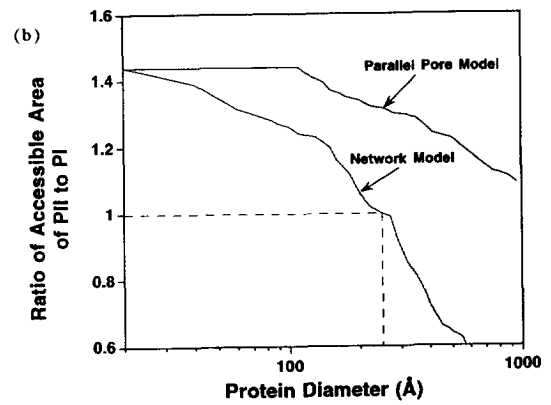

Fig. 10. Ratio of accessible areas for POROS II to POROS I for different protein sizes. (a) Comparison between experimental and simulation data; (●) experimental data, (line) model simulation. (b) Comparison between network model and parallel pore model.

comparison, the simulated data for the bundle of a parallel-tube model are also shown. From Fig. 10a, it can be seen that the match between experimental and simulation data (network model) is excellent. More importantly, these results demonstrate the important role that the pore interconnectivity plays in surface area accessibility in the porous structure of the media (Fig. 10b). With a parallel-pore model where there is no interconnectivity, solute molecules can access the pores in the particle uninterrupted, and the ratio of the accessible areas remains almost constant up to a solute diameter of about 100 Å.

The other important observation from the simulation data is that with a solute diameter of about 250 Å, there does not seem to be a competitive advantage of POROS I over POROS II in terms of extra surface area for protein adsorption. This is because with such a large solute, a significant portion of the surface area in POROS II cannot be accessed due to the shielding of the pores which contribute to surface area for adsorption by other, smaller pores in the interconnected porous medium.

7.6. Size-exclusion chromatography

Apart from being able to predict experimental data based on surface area accessibility, the network model can also elucidate experimental data based on volume accessibility. For this, size-exclusion chromatography was simulated using the model, and the data compared with the experimental results. Fig. 11 shows a comparison between simulated and experimental data for the partition coefficient, K, as a function of the gyration diameter of the polystyrene molecules for POROS I and II. The agreement between the simulated and experimental data is excellent. For POROS I, errors between the two sets of data vary from 4% to 10%, while for POROS II, they range from 5% to 7%. The excellent agreement of the data indicates that the discrete network model can offer a useful approach for the specification and design of column media for SEC applications.

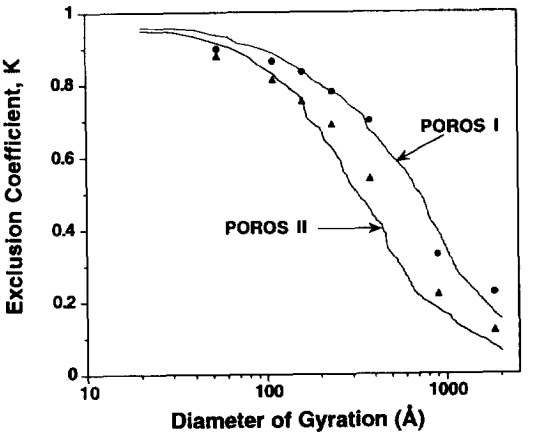

Fig. 11. Size-exclusion chromatography for POROS I and POROS II. (●) POROS I, experimental data; (▲) POROS II, experimental data.

8. Conclusions

The lattice network model established can be used to infer the parameters of the pore-size distribution and pore interconnectivity, describing the porous structure of the particles by simulating mercury porosimetry experiments on the network. Sensitivity analyses carried out optimized the lattice size and ascertained the uniqueness of the input parameters obtained. The results indicate that the PSD of POROS packings comprises a group of macropores (1000 Å range) and a group of micropores (100 Å range), which is consistent with measurements inferred from SEM. The established model provides a useful tool for obtaining the PSD of porous materials when other methods such as mercury porosimetry involves erroneous data interpretation and TEM and densitometry measurements may not be conveniently applied without appropriate staining protocol and hence are too laborious. Using the model, the pore number distribution has been discretized on a per particle or per particle volume basis, which can provide a simple comparison of the PSDs between different perfusive materials.

Mercury intrusion has been simulated using the model on blends of POROS I and II. The excellent agreement between simulation and experimental data not only provided a validation

of the network, but it also confirms the PSD parameters obtained for POROS I and II. This is also an indication that the model can be used as a quality control/assurance tool.

By simulating the adsorption capacities for proteins of varying sizes on POROS I and II materials, the network model can be used to study the accessible porous surface area available for adsorption. The results have demonstrated the importance of pore interconnectivity for the accessibility of the porous structure by a comparison of the accessible surface area for the network model against a parallel-pore model whereby the pores are not connected to each other. It has also been shown from the simulations that there is no competitive advantage of POROS II over POROS I, in terms of adsorption capacity, when the solute molecule exceeds a critical size. In that case, accessibility to the pores in POROS II can be decreased due to pore interconnectivity, in which case pores which provide the surface area are shielded by smaller pores nearer the surface. Experimentally, SEC has been performed using polystyrene standards of small polydispersities. Principles of statistical mechanics and Monte Carlo techniques have been employed to provide the framework for steric exclusion of flexible macromolecules in the pores. The agreement between simulation and experimental data indicates that the model can be used to simulate SEC.

Acknowledgements

The authors wish to acknowledge the financial support from the National University of Singapore for its fellowship (to K.-C. Loh) and the support from the National Science Foundation under the Engineering Research Center Initiative to the Biotechnology Process Engineering Center under the cooperative agreement EEC-88-03014.

References

[1] N.B. Afeyan, N.F. Gordon, I. Mazsaroff, L. Varady, S.P. Fulton, Y.B. Yang and F.E. Regnier, J. Chromatogr., 519 (1990) 1.
[2] G. Carta and A.E. Rodriguez, Chem. Eng. Sci., 48 (1993) 3927.
[3] D.D. Frey, E. Schweinheim and C. Horvath, Biotech. Prog., 9 (1993) 273.
[4] A.I. Liapis and M.A. McCoy, J. Chromatogr., 599 (1987) 87.
[5] A.E. Rodriguez, Z.P. Lu and J.M. Laureiro, Chem. Eng. Sci., 46 (1991) 2765.
[6] A.E. Rodriguez, Z.P. Lu, J.M. Loureiro and G. Carta, J. Chromatogr. A, 653 (1993) 189.
[7] N. Tanaka, K. Kimata and T. Araki, J. Chromatogr., 544 (1991) 319.
[8] F.A.L. Dullien, POROS MEDIA: Fluid Transport and Pore Structure, 2nd ed., Academic Press, New York, 1992.
[9] N. Tanaka, K. Kimata, K. Hosoya, T. Araki, H. Tsuchiya and K. Hashizume, J. High Resolut. Chromatogr., 14 (1991) 40.
[10] G.P. Androutsopoulos and R. Mann, Chem. Eng. Sci., 33 (1978) 673.
[11] A.O. Imdakm and M. Sahimi, Chem. Eng. Sci., 46 (1991) 1977.
[12] R.L. Portsmouth and L.F. Gladden, Chem. Eng. Sci., 46 (1991) 3023.
[13] S.D. Rege and H.S. Fogler, AIChE J., 34 (1988) 1761.
[14] A.M. Lane, N. Shah and W.C. Conner, J. Colloid Interface Sci., 109 (1986) 235.
[15] G.R. Lapidus, A.M. Lane, K.M. Ng and W.C. Conner, Chem. Eng. Commun., 38 (1985) 33.
[16] W.C. Conner, A.M. Lane, K.M. Ng and M. Goldblatt, J. Catal., 83 (1983) 336.
[17] R. Mann, J.J. Almeida and M.N. Mugerwa, Chem. Eng. Sci., 41 (1986) 2663.
[18] C.D. Tsakiroglou and A.C. Payatakes, in Rodriguez-Reinoso et al. (Editors), Characterization of Porous Solids II, Elsevier Science Publishers, London, 1991, pp. 169–178.
[19] M.P. Hollewand and L.F. Gladden, Chem. Eng. Sci., 47 (1992) 1761.
[20] S.D. Rege and H.S. Fogler, Chem. Eng. Sci., 42 (1987) 1553.
[21] M. Sahimi, G.R. Gavalas and T.T. Tsotsis, Chem. Eng. Sci., 45 (1991) 1443.
[22] K. Unger and M.G. Gimpel, J. Chromatogr., 180 (1979) 93.
[23] H. Colin and G. Guichon, J. Chromatogr., 126 (1976) 43.
[24] E. Tracz, R. Leboda and E. Mizera, J. Chromatogr., 355 (1986) 412.
[25] E. Tracz, J. Skubiszewska and R. Leboda, J. Chromatogr., 287 (1984) 136.
[26] K.C. Loh, Ph.D. Thesis, Massachusetts Institute of Technology, Cambridge, MA, 1995.
[27] D. Stauffer, Introduction to Percolation Theory, Taylor and Francis, London, 1985.
[28] S.K. Park and W.M. Keith, Commun. ACM, 31 (1988) 1192.
[29] I. Fatt, Petrol. Trans. AIME, 207 (1956) 144.
[30] W. Rose, Illinois State Geological Survey Circular, 237 (1957) 1.

[31] L.L. Havilcek and R.D. Crain, Practical Statistics for the Physical Sciences, ACS Professional Reference Book, American Chemical Society, Washington, DC, 1988, p. 212.
[32] A.M. Lane, Ph.D. Thesis., University of Massachusetts, 1983.
[33] J.C. Giddings, E. Kucera, C.P. Russell and M.N. Myers, J. Phys. Chem., 72 (1968) 4397.
[34] J.H. Knox and H.P. Scott, J. Chromatogr., 316 (1984) 311.
[35] E.F. Casassa, J. Polym. Sci. Part A-2, 10 (1972) 381.
[36] M.G. Davidson, U.W. Suter and W.M. Deen, Macromolecules, 20 (1987) 1141.
[37] M.E. van Krefeld and N. van den Hoed, J. Chromatogr., 83 (1973) 111.
[38] L.K. Frevel and L. Kessley, J. Anal. Chem., 35 (1963) 1492.
[39] R.P. Mayer and R.A. Stowe, J. Colloid. Sci., 20 (1965) 893.
[40] D.M. Smith and D.L. Stermer, Powder Technol., 53 (1987) 23.